AFRL-RV-PS-
TR-2022-0073

AFRL-RV-PS-
TR-2022-0073

SEMICONDUCTOR DEVICE TECHNOLOGIES FOR SPACE APPLICATIONS

Ganesh Balakrishnan

University of New Mexico
1700 Lomas Blvd NE
Albuquerque, NM 87106

30 Jun 2020

Final Report

APPROVED FOR PUBLIC RELEASE; DISTRIBUTION IS UNLIMITED.

AIR FORCE RESEARCH LABORATORY
Space Vehicles Directorate
3550 Aberdeen Ave SE
AIR FORCE MATERIEL COMMAND
KIRTLAND AIR FORCE BASE, NM 87117-5776

NOTICE AND SIGNATURE PAGE

Using Government drawings, specifications, or other data included in this document for any purpose other than Government procurement does not in any way obligate the U.S. Government. The fact that the Government formulated or supplied the drawings, specifications, or other data does not license the holder or any other person or corporation; or convey any rights or permission to manufacture, use, or sell any patented invention that may relate to them.

This report is the result of contracted fundamental research which is exempt from public affairs security and policy review in accordance with AFI 61-201, paragraph 2.3.5.1. This report is available to the general public, including foreign nationals. Copies may be obtained from the Defense Technical Information Center (DTIC) (http://www.dtic.mil).

AFRL-RV-PS-TR-2022-0073 HAS BEEN REVIEWED AND IS APPROVED FOR PUBLICATION IN ACCORDANCE WITH ASSIGNED DISTRIBUTION STATEMENT.

//SIGNED//

PRESTON WEBSTER
Program Manager

//SIGNED//

CHRISTIAN MORATH
Tech Advisor, Space Control Technologies Branch

//SIGNED//

JOHN BEAUCHEMIN
Chief Engineer, Spacecraft Technology Division
Space Vehicles Directorate

This report is published in the interest of scientific and technical information exchange, and its publication does not constitute the Government's approval or disapproval of its ideas or findings.

Approved for public release; distribution is unlimited.

REPORT DOCUMENTATION PAGE

Form Approved
OMB No. 0704-0188

1. REPORT DATE *(DD-MM-YYYY)*	**2. REPORT TYPE**	**3. DATES COVERED** *(From - To)*
30-06-2022	Final Report	09-19-2019- 30-06-2022

4. TITLE AND SUBTITLE

Semiconductor Device Technologies for Space Applications

5a. CONTRACT NUMBER
FA9453-19-2-0015

5b. GRANT NUMBER

5c. PROGRAM ELEMENT NUMBER
61102F

6. AUTHOR(S)

Ganesh Balakrishnan

5d. PROJECT NUMBER
3001

5e. TASK NUMBER
EF133067

5f. WORK UNIT NUMBER
V1FE

7. PERFORMING ORGANIZATION NAME(S) AND ADDRESS(ES)
University of New Mexico
1700 Lomas Blvd NE
Albuquerque, NM 87106

8. PERFORMING ORGANIZATION REPORT NUMBER

9. SPONSORING / MONITORING AGENCY NAME(S) AND ADDRESS(ES)
Air Force Research Laboratory
Space Vehicle Directorate
3550 Aberdeen Ave SE
Kirtland Air Force Base, NM 87117-5776

10. SPONSOR/MONITOR'S ACRONYM(S)
AFRL/RVSU

11. SPONSOR/MONITOR'S REPORT NUMBER(S)
AFRL-RV-PS-TR-2022-0073

12. DISTRIBUTION / AVAILABILITY STATEMENT

Approved for public release; distribution is unlimited.

13. SUPPLEMENTARY NOTES

14. ABSTRACT

In collaboration with AFRL Space Vehicles Directorate, this effort seeks to investigate
1 Development of epitaxial techniques and approaches to realize novel platforms for infrared detectors.
2 Ultrafast laser optical experiments and modeling of ultrafast carrier dynamics.
3 Advanced characterization methods for investigating IR detector materials.
4 Modelling of sensors.

15. SUBJECT TERMS
IR sensors, infrared sensors, InAsSbBi, molecular beam epitaxy, ultrafast

16. SECURITY CLASSIFICATION OF:			**17. LIMITATION OF ABSTRACT**	**18. NUMBER OF PAGES**	**19a. NAME OF RESPONSIBLE PERSON**
a. REPORT	**b. ABSTRACT**	**c. THIS PAGE**			Preston Webster
Unclassified	Unclassified	Unclassified	SAR	32	**19b. TELEPHONE NUMBER**

(This Page Intentionally Left Blank)

TABLE OF CONTENTS

LIST OF FIGURES

Page

LIST OF TABLES

Page

(This Page Intentionally Left Blank)

1.0 SUMMARY

The effort in the past year involved working closely with AFRL Space Vehicles Directorate to develop molecular beam epitaxy (MBE) capabilities for narrow bandgap semiconductor alloys. Alloys based on bismuth and metamorphic buffers have been explored in depth with some state-of-the-art results in both systems. A series of InAsSbBi growths with varying bismuth percentages and growth temperatures were realized. In addition to this high quality InGaAsSbBi was also realized. These alloys have been characterized using time resolved photoluminescence, cryogenic photoluminescence, X-Ray diffraction. The growths reported as some of the highest quality bismuth alloys reported to date across metrics.

2.0 INTRODUCTION

Narrow gap antimonides have been of significant interest to the Air Force for detector applications. The latest advancements in this area of research involves the growth of bismuth based III-Vs that can be grown lattice matched on GaSb substrates. The primary issue with this growth process is the incorporation of bismuth into alloys such as InAsSbBi and InGaAsSbBi. The large bismuth atom tends to segregate and form surface clusters. However, through various growth conditions used in molecular beam epitaxy (MBE) such as growth temperatures and III-V ratios, it is possible to achieve dilute bismuth III-V alloys. These alloys need to be characterized for photoluminescence and carrier lifetime to determine their suitability for detector applications. In this project we have worked on the development of a MBE reactor specifically for use with bismuth. We have also grown, in collaboration with the AFRL Space Vehicles Directorate a series of dilute bismuth alloys with excellent bismuth incorporation and some of the best reported lifetimes.

3.0 METHODS, ASSUMPTIONS, AND PROCEDURES

The method for fabricating the epitaxial samples in this project is solid source molecular beam epitaxy. The process involves the use of an ultra-high vacuum (UHV) chamber in which effusion cells are used to evaporate group III and group V elements onto a substrate. The reactor used is a VG V80 dual chamber system. It has Veeco ® Sumo effusion cells for group III alloys and valved crackers for the arsenic and antimony sources. The characterization of the samples for crystallographic quality is done using x-ray diffraction. The alloys are also optically characterized using phase contrast microscopy and electron microscopy including scanning electron microscopy and energy dispersive spectroscopy. Finally, a comprehensive photoluminescence analysis of the samples is done using both cryogenic photoluminescence and time-resolved photoluminescence.

4.0 RESULTS AND DISCUSSION

4.1 Technological leap in optoelectronic quality of InAsSbBi

The contents of this section are discussed in greater detail in our publication [1].

Four InAsSbBi samples are grown on (100)-oriented *n*-type GaSb substrates using a VG-V80H molecular beam epitaxy (MBE) system with valved group-V sources. The InAsSbBi samples consist of a 1 μm thick active region of InAsSbBi, sandwiched between 100 nm and 400 nm layers of lattice-matched InAsSb, which provide a small degree of carrier confinement for photoexcited electron hole pairs. The sample cross-section is shown in the inset of Fig. 1. The samples are grown at an In-limited growth rate of 1.0 μm/hour at 360 or 380 °C for the InAsSbBi layer. These conditions produce Bi mole fractions ranging from 0.002 to 0.008 and Sb mole fractions ranging from 0.077 to 0.09 in InAsSbBi, yielding nearly lattice-matched materials. The InAsSb buffer and cap, however, are grown at 440 °C to preserve the quality of the InAsSb buffer on which each InAsSbBi layer is grown, and to ensure that the 100 nm cap is of high quality with no unintentional Bi content in order to provide effective confinement of photogenerated carriers from the surface.

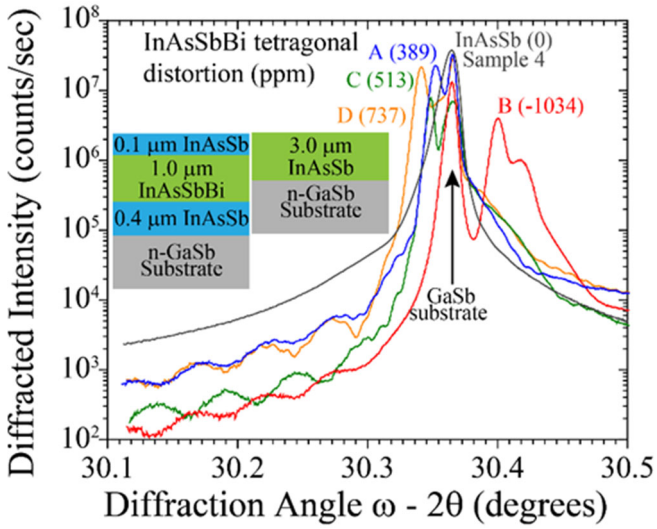

Figure 1. X-ray diffraction from bulk InAsSb and InAsSbBi samples on GaSb. Parentheses give the tetragonal distortion inferred from the substrate-layer peak separation, in units of parts per million. Inset shows InAsSbBi and InAsSb sample cross-sections

A set of four InAsSb samples, lattice-matched to GaSb substrates, are grown at temperatures between 350 and 440 °C for comparison to the InAsSbBi samples, summarized in Table 1. The InAsSb samples consist of a 3 μm thick layer of InAsSb on a GaSb substrate, intentionally grown thicker than the 1 μm thick InAsSbBi samples to partially compensate for the lack of carrier confinement and to enable more careful examination of surface morphology at lower growth temperatures. The sample cross-

section is also included in the inset of Fig. 1. Nomarski microscopy is used to evaluate the surface morphology of all the samples under 20× magnification, and the surfaces are determined to be smooth and droplet-free.

Table 1. Growth temperatures, tetragonal distortions, bandgap energies, and Sb and Bi mole fractions of InAsSb and InAsSbBi samples

Sample	Growth Temp (°C)	Tetragonal Distortion (ppm)	E_g at 120 K (meV)	Sb Mole Fraction	Bi Mole Fraction
InAsSb (1)	350	789	299	0.095	0.000
InAsSb (2)	380	626	299	0.094	0.000
InAsSb (3)	410	0	303	0.090	0.000
InAsSb (4)	440	0	309	0.090	0.000
InAsSbBi (A)	380	389	306	0.090	0.002
InAsSbBi (B)	380	-1034	304	0.077	0.004
InAsSbBi (C)	380	513	298	0.082	0.005
InAsSbBi (D)	360	737	281	0.081	0.008

The (004) lattice plane X-ray diffraction patterns of the four InAsSbBi samples (samples A – D) and one lattice-matched InAsSb sample grown at an optimal temperature of 440 ºC (sample 4) are shown in Fig. 1 and are used to determine the tetragonal distortion in the InAsSbBi. The peak from the GaSb substrate is indicated along with the peaks from the InAsSbBi layer in the various samples, all of which exhibit strong Pendellösung fringes indicative of high-quality smooth layer interfaces. When the layer strain is small, the tetragonal distortion is described to the first order by Equation 1 [2,3].

$$\varepsilon_{\perp} = -\frac{\theta_{InAsSbBi} - \theta_{GaSb}}{\tan(\theta_{GaSb})} \quad (1)$$

The tetragonal distortion of the InAsSbBi layer in each sample is given in units of ppm in parentheses in Fig. 1 and in Table 1. By comparing this lattice distortion with the bandgap energy extracted from photoluminescence measurements, the Bi and Sb mole fractions are obtained [4]. Reciprocal space maps confirm that all of the lattice-matched and slightly-compressive samples are pseudomorphic, whereas the one tensile sample (Sample B) is partially relaxed. As a result, the strain and composition analysis of Sample B is only approximate.

Photoluminescence is measured from the InAsSb(Bi) samples using a Bruker 80V Fourier transform infrared spectrometer and a 785-nm wavelength pump laser. The double modulation technique is utilized to increase the signal to noise ratio [5], with the laser modulated at a frequency of 50 kHz. The steady-state low temperature (120 K) photoluminescence spectra of the bismide samples are shown in Fig. 2, along with the spectrum of InAsSb sample 4 for comparison. Though the 100 nm thick InAsSb cap parasitically absorbs some of the 785-nm wavelength pump laser radiation in the InAsSbBi samples, the hole mobility for InAsSb is determined to be 1186 cm^2/Vs [6], while the minority carrier lifetime for InAsSb grown at 440 °C is demonstrated later in this work

and found to be approximately 1 μs. Based on these values, the minority hole diffusion length is calculated to be 28 μm at 77 K from Equation 2,

$$L_h = \sqrt{\mu_h \tau_h \mathrm{kT}/e} \quad (2)$$

where μ_h is the hole mobility, τ_h is the minority carrier lifetime, k is the Boltzmann constant, T is the temperature, and e is the charge of an electron. As the InAsSb diffusion length is much greater than the 100 nm thickness of the cap, electron-hole pairs generated there that do not immediately recombine at the surface are expected to predominately diffuse into and recombine in the lower-bandgap lower-lifetime InAsSbBi region. To further verify that the measured photoluminescence is from the InAsSbBi absorber region, in one instance the InAsSb cap of bismide sample C is etched down to approximately 35 nm, for the purpose of significantly reducing any potential photoluminescence from the cap while still offering some isolation from surface recombination. The photoluminescence spectra and bandgap energies for both the etched and unetched samples C are found to be approximately the same, indicating that the photoluminescence is indeed from the bismide layer. The photoluminescence peak of the GaSb substrate is not measurable for the bismide samples, due to minimal pump light reaching the substrate at low excitation powers.

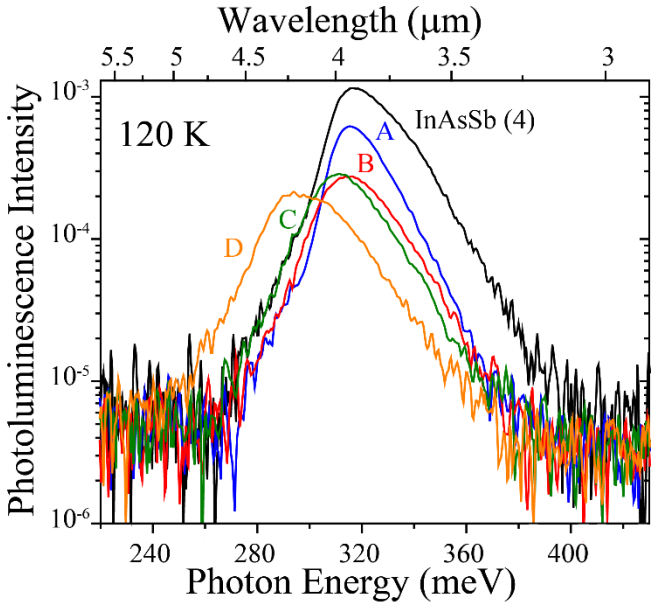

Figure 2. Photoluminescence from InAsSbBi and InAsSb samples at 120 K, showing wavelength extension and Urbach slope increase due to the addition of Bi in InAsSb

The bandgap energy of each sample in Fig. 3 is identified at the maximum of the photoluminescence spectra's first derivative [7], which identifies the onset of the continuum states at the band edge. This first derivative evaluation enables accurate determination of the bandgap energy without influence of the Urbach tail slope, which is a function of the growth conditions. Lower peak intensities and extension of the photoluminescence first derivative maxima and peak positions of the bismide samples to wavelengths longer than that of InAsSb with the same degree of strain provide evidence

that this luminescence is emitted by the InAsSbBi. The Bi and Sb mole fractions of each of the InAsSbBi and InAsSb samples, along with their respective growth temperatures, tetragonal distortions, and bandgaps at 120 K, are provided in Table 1.

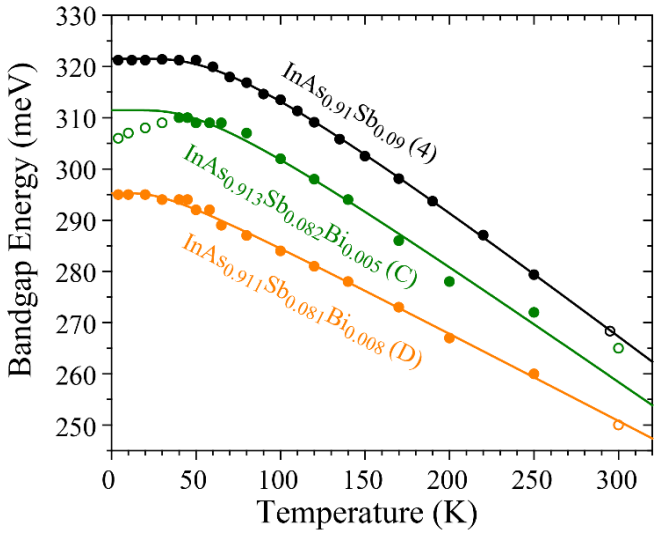

Figure 3. Bandgap energy of $InAs_{0.91}Sb_{0.09}$, $InAs_{0.913}Sb_{0.082}Bi_{0.005}$, and $InAs_{0.911}Sb_{0.081}Bi_{0.008}$ as a function of temperature (solid circles), with Einstein single oscillator model fits (solid curves). Hollow circles are excluded from the fit, and are representative of photoluminescence from localized states (Sample C: 4 to 30 K) and noisier photoluminescence at a high temperature (Samples 4, C, and D: 295 to 300 K)

Temperature-dependent photoluminescence measurements are taken from 4 K to 300 K to analyze the bandgap energy as a function of temperature. The temperature-dependent bandgap is included in Fig. 3 for bulk InAsSb sample 4 ($InAs_{0.91}Sb_{0.09}$) and InAsSbBi samples C ($InAs_{0.913}Sb_{0.082}Bi_{0.005}$) and D ($InAs_{0.911}Sb_{0.081}Bi_{0.008}$). The temperature dependence of the bandgap energy is evaluated using the Einstein single oscillator model [7-9] in Equation 3,

$$E_g = E_0 - \frac{S_0 k T_E}{\exp\left(\frac{T_E}{T}\right) - 1} \tag{3}$$

where E_0 is the bandgap energy at 0 K, S_0 is the electron-phonon coupling strength, k is the Boltzmann constant, and T_E is the Einstein temperature. The best-fit parameters for bulk InAsSb sample 4 and bismide samples C and D are included in Table 2.

Table 2. Einstein single oscillator model fit parameters for InAsSb sample 4 and InAsSbBi samples C and D

Sample	E_0 (meV)	S_0	T_E (K)
InAsSb (4)	321.5	2.94	192.1
InAsSbBi (C)	311.5	2.69	154.7
InAsSbBi (D)	295.3	1.99	86.3

The bandgap energies at 120 K for InAsSb sample 4 and bismide samples C and D are found to be 309 meV (4.01 μm), 298 meV (4.16 μm), and 281 meV (4.41 μm), respectively. The results in Fig. 3 indicate that as the bismuth mole fraction is increased from $InAs_{0.91}Sb_{0.09}$ to $InAs_{0.913}Sb_{0.082}Bi_{0.005}$ to $InAs_{0.911}Sb_{0.081}Bi_{0.008}$, the bandgap energy decreases across all measurement temperatures. The bandgap energy of Sample C, or $InAs_{0.913}Sb_{0.082}Bi_{0.005}$, exhibits a blue shift to higher energies between 4 and 40 K, before returning to the traditional bandgap temperature dependence from 40 K to 300 K. This may be attributed to radiative recombination from localized band tail states at low temperatures, which has been previously reported in some InAsSbBi and GaAsBi samples [4,10-13]. However, Sample D with 0.8% Bi did not exhibit this property, indicating that these states may have some growth condition dependence that can be mitigated.

Time-resolved photoluminescence measurements are also performed on the InAsSbBi and InAsSb samples in order to determine their minority carrier lifetimes. A pulsed 1535-nm laser, with 3.5 ns pulse widths, is used to excite the samples, while a half waveplate in conjunction with a polarizing beamsplitter is used to attenuate the laser to produce low injection conditions in the material. The photoluminescence decays at low pump powers for InAsSbBi samples C and D and InAsSb samples 2 and 4 are shown in Fig. 4a at 120 K. The low pump power excitation conditions are 1.6×10^{11} photons/cm^2 per pulse for all of the InAsSb samples; 2.2×10^{11} photons/cm^2 per pulse for bismide samples A, B, and C; and 3.1×10^{11} photons/cm^2 per pulse for bismide sample D. These conditions are determined by measuring the laser power per unit area outside the cryostat to obtain the photon flux, which is modified to account for reflection and absorption at the cryostat's CaF_2 window and the sample's cap layer (when present) using optical constants taken from the Handbook of Optical Constants [14].The handbook does not have optical constants for InAsSb, but they are estimated by shifting the optical constants of InAs by 75 meV to the known bandgap energy of lattice-matched InAsSb. This yields an estimated absorption coefficient of 2.36×10^4 cm^{-1} and a corresponding parasitic loss of about 20% of the 1535 nm wavelength pump excitation in the 100 nm thick InAsSb cap (when present). For the InAsSb samples, when distributed over the 3 μm active region, the result is an excitation of approximately 5.33×10^{14} electron-hole pairs per cm^3, which is comparable with the previously reported background density for this material system, indicating near-low injection conditions [15,16]. When distributed over the 1 μm active region for the bismide samples, the two excitation conditions yield approximately 2.2×10^{15} and 3.1×10^{15} electron-hole pairs per cm^3, respectively, and are also near the cutoff of the low injection regime, which is evident by the pure single exponential decays observed in Fig. 4a [17].

To again ensure that the observed photoluminescence is from the InAsSbBi absorber region rather than the InAsSb cap, time-resolved photoluminescence is also measured using a 3.2-μm laser, which will have almost an order of magnitude larger penetration depth into the samples than the 1535-nm laser. Despite the very different excitation profile, the overall intensity of the photoluminescence decay and the minority carrier lifetimes extracted from the time-resolved photoluminescence performed with the 3.2-μm laser are consistent with those of the 1535-nm pump laser, indicating that the measured photoluminescence is largely from the bismide layer, and not the InAsSb cap. If anything,

recombination in the InAsSb cap may slightly decrease the measured lifetime, possibly as a result of surface recombination. Thus, the extracted lifetimes for the InAsSbBi should be considered a conservative lower bound. Additionally, it is expected that the photon recycling factor should be fairly low (approximately 1.35) given the thicknesses of the cap, absorber, and buffer regions, and should therefore not have a significant impact on the minority carrier lifetime [18].

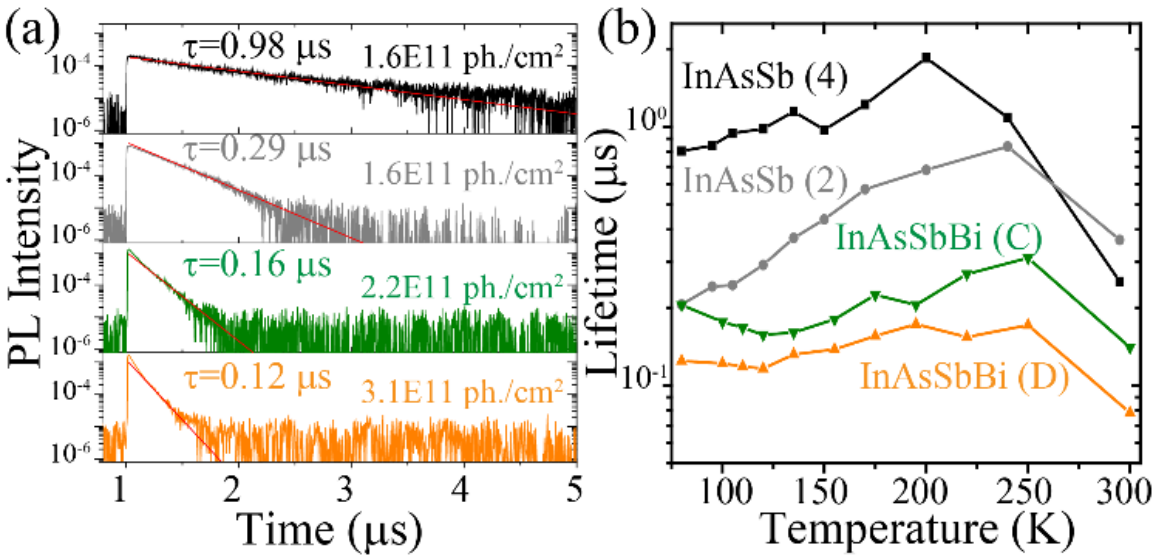

Figure 4. (a) Time-resolved photoluminescence decays of InAsSb samples 4 and 2 and bismide samples C and D at 120 K. (b) Minority carrier lifetimes of samples 4, 2, C, and D as a function of temperature

The time-resolved photoluminescence decay data is fit to a single exponential (solid red line) to determine the minority carrier lifetimes plotted as a function of temperature in Fig. 4b. The resulting lifetimes for InAsSb sample 4 in Fig. 4b demonstrate that the growth chamber is capable of producing high-quality lattice-matched InAsSb with lifetimes exceeding 1 μs. Under higher excitation conditions a longer decay tail begins to manifest in all of the shorter lifetime bismide samples grown at lower temperatures, which may be the result of increasing luminescence from the more localized states in the Urbach tail of the band edge or from elsewhere in the structure, such as the underlying InAsSb or substrate layers. However, the lifetimes reported are measured under low pump power excitation conditions.

The minority carrier lifetimes of both the InAsSb (squares) and InAsSbBi (circles) samples measured at 120 K are plotted as a function of growth temperature in Fig. 5 for their respective lowest excitation conditions, with error bars reflecting the uncertainty in the chosen fit windows. The lifetime data for the InAsSb samples, for these low pump-power conditions, is also fit to a single exponential. The growth parameters (growth temperatures and flux ratios) and the minority carrier lifetimes at 120 K for each sample are presented in Table 3.

Table 3. Growth temperatures, flux ratios, and minority carrier lifetimes at 120 K of InAsSb and InAsSbBi samples

Sample	Growth Temp (°C)	As/In Flux Ratio	Sb/In Flux Ratio	Bi/In Flux Ratio	Minority Carrier Lifetime (μs): 120 K
InAsSb (1)	350	1.2	0.1	0	0.095
InAsSb (2)	380	1.2	0.1	0	0.29
InAsSb (3)	410	1.2	0.1	0	0.47
InAsSb (4)	440	1.2	0.1	0	0.98
InAsSbBi (A)	380	1.16	0.085	0.03	0.21
InAsSbBi (B)	380	1.13	0.085	0.06	0.14
InAsSbBi (C)	380	1.16	0.069	0.06	0.16
InAsSbBi (D)	360	1.14	0.081	0.06	0.12

Fig. 5 shows that the minority carrier lifetimes of both the InAsSb and InAsSbBi samples decrease as growth temperature is decreased. The InAsSbBi samples have comparable, though slightly lower, minority carrier lifetimes than the InAsSb samples grown at the same temperatures, which may be due to the slightly leaner As flux conditions utilized to facilitate the incorporation of Bi. Nonetheless, bismide sample A grown at 380 °C has a minority carrier lifetime of 0.21 μs. This value is only slightly lower than the experimentally measured lifetime of 0.29 μs for InAsSb sample 2. Sample D, which is grown at 360 °C, has a minority carrier lifetime of 0.12 μs at 120 K, while an interpolation of the InAsSb lifetime data suggests that an InAsSb sample grown at 360 °C would be expected to have a lifetime of 0.16 μs. Sample B exhibits the lowest minority carrier lifetime at 380 °C, most likely due to the noted partial relaxation in this sample, and overall, the lifetimes for the bismide samples grown at 380 °C appear to increase as the magnitude of the tetragonal distortion decreases. These results indicate that the minority carrier lifetimes of the bismide samples follow the InAsSb trend in Fig. 5 as a function of growth temperature, suggesting that the incorporation of bismuth itself does not negatively impact the minority carrier lifetime. However, the lower growth temperatures (360 – 380 °C) required to effectively incorporate Bi do seem to adversely affect the optical qualities of the material. Nevertheless, substantial Bi mole fractions on the order of 1% are achieved with smooth surface morphology and technologically-relevant minority carrier lifetimes, indicating that future work should endeavor to identify growth conditions that enable this level of Bi incorporation at higher growth temperatures.

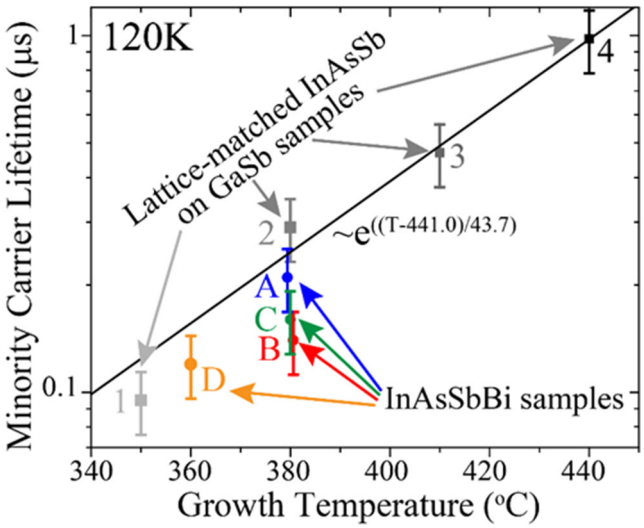

Figure 5. Minority carrier lifetime of lattice-matched InAsSb (squares) and InAsSbBi (circles) as a function of growth temperature

4.2 Enhancing Bi incorporation while retaining high quality in GaInAsSbBi

The contents of this section are discussed in greater detail in our publication [19].

In order to evaluate GaInAsSbBi as a candidate for mid-wave infrared detection, a sufficient quantity of Bi should be incorporated to achieve a 5 μm wavelength cutoff, (~2% Bi mole fraction for a 120 K operating point, InAsSb has a 3 μm cutoff for comparison). [20,3] Fundamental optoelectronic quality metrics such as the alloy's minority carrier lifetime τ_{mc} need to be investigated. The minority carrier lifetime is a strong function of the growth conditions utilized during the material's growth, with particularly strong dependence on the growth temperature. [21] Low growth temperatures below 350 ºC have traditionally been utilized to facilitate more efficient Bi incorporation in InAsBi and InAsSbBi; [20,3] however, photoluminescence has yet to be observed in thick bulk layers grown under these conditions. In contrast, InAsSbBi grown at higher temperatures (between 360 and 380 ºC) exhibits strong photoluminescence and minority carrier lifetimes comparable to equivalent InAsSb samples grown at the same temperatures (~100's of ns). However Bi incorporation is severely reduced at these temperatures (~0.2-0.5% mole fraction incorporated to date), [1] and Bi incorporation efficiency will be further reduced at temperatures > 400 ºC where the longest lifetimes can likely be achieved. [22] This leaves InAsSbBi in a compromised position where it is difficult to simultaneously achieve sufficient Bi incorporation to reach a 5 μm mid-wave infrared cutoff while maintaining a technologically relevant minority carrier lifetime (> 1 μs).

The addition of Ga in GaInAsSbBi may present a solution to this impasse in InAsSbBi. GaAsBi with ~1% mole fraction of Bi has been grown at 400 °C, and higher Bi incorporation rates have been demonstrated at similar temperatures. [23,24] This suggest that Bi forms a stronger bond to Ga than to In at ~400 ºC growth temperatures, possibly due to Ga's smaller atomic radius, which lends itself to an increase in atomic orbital overlap. Thus, co-alloying Bi with Ga could result in a lower alloy formation energy and better dilute Bi incorporation efficiency as a result. [25] Here, we demonstrate a quinary GaInAsSbBi alloy grown at 400 °C by molecular beam epitaxy which achieves the same cutoff wavelength due to Sb and Bi incorporation as a quaternary InAsSbBi alloy grown under similar flux conditions at 360 °C. The quinary's substantially longer minority carrier lifetime is consistent with the higher growth temperature. The structural and optical properties are examined by Nomarski interference contrast microscopy, X-ray diffraction, Rutherford backscattering spectroscopy, steady-state photoluminescence, and time-resolved photoluminescence. A recombination rate analysis is performed on the temperature dependent minority carrier lifetime to determine the intrinsic doping density of the quinary GaInAsSbBi and quaternary GaInAsSb reference.

The samples are grown on (100)-oriented *n*-type GaSb substrates using a VG-V80H molecular beam epitaxy system with valved group-V sources. The growth temperatures is measured using a Fluke Endurance series emissivity-corrected pyrometer, model E2ML sensing at 1.6 μm with a minimum temperature limit of 250 °C. The emissivity setting is 0.655, calculated using the refractive index of GaSb. The quaternary and quinary GaInAsSb(Bi) samples are sandwiched between a 500 nm thick buffer and a

30 nm thick cap of lattice matched InAsSb. The 30 nm thickness of the cap layer is chosen so that it is sufficiently thick to provide confinement to photogenerated carriers, yet thin enough to produce a spectral range which is uniquely characteristic of Bi in the Rutherford backscattering yield spectrum. The quaternary InAsSbBi sample from Ref. [1] was sandwiched between a 400 nm thick buffer and a 100 nm cap of lattice matched InAsSb.

Before a quinary is grown with desired constituent mole fractions, group-III growth rates and V/III flux ratios are calibrated, [26] followed by three alloy composition calibration growths. The first calibration is a lattice-matched InAsSb layer grown at 440 °C with an In-limited growth rate of 1 μm/hr, an As/In flux ratio of ~1.4, and an Sb/In flux ratio of ~0.11 to achieve lattice-match on the GaSb substrate and produce a high quality InAsSb reference. These growth conditions are repeated for the second composition calibration, with the growth temperature reduced to 400 °C and As/In flux ratio reduced to near unity, resulting in increased Sb incorporation and intentionally compressive InAsSb. Next, Ga is introduced in the third composition calibration with a target 0.027 μm/hr Ga growth rate and 0.973 μm/hr In growth rate to compensate the compressive strain, producing lattice-matched GaInAsSb. The total group-III growth rate target is 1 μm/hr so that the Sb/III and As/III flux conditions are maintained. Finally, the lattice-matched quaternary GaInAsSb is grown again, but with the addition of Bi to grow quinary GaInAsSbBi. Table 4 summarizes the growth conditions and the (004) layer-substrate peak separation (in arcseconds) of each layer measured by X-ray diffraction.

Table 4. Summary and growth conditions of the calibration InAsSb and GaInAsSb, and quinary GaInAsSbBi samples

Sample	Growth Temp. (°C)	Strain (arcsec)	Growth rates (μm/hr)		Flux Ratios		
			In	Ga	As/III	Sb/III	Bi/III
InAsSb	400	-462	1.008	0	0.953	0.110	0
GaInAsSb	400	-22	0.969	0.029	0.963	0.112	0
GaInAsSbBi	400	-54	0.985	0.029	0.966	0.108	≈0.02

Smooth, droplet free surfaces are observed for all samples with Normarski imaging. The inset to Fig.6 shows the Rutherford backscattering spectroscopy yield signal (red curve), and the backscattering model fit of 0.13% ± 0.02% Bi mole fraction in the GaInAsSbBi sample (black curve) leading to a predicted 7.15 meV redshift in bandgap. To maximize RBS sensitivity to Bi, a 5 MeV Fe3+ beam is employed. An annular partially depleted silicon surface barrier detector is placed at 180 degrees and approximately 5 μC of charge is accumulated for both the reference and quinary samples at room temperature. Fig. 6 shows the (004) X-ray diffraction pattern of the GaInAsSb sample which exhibits -22” compressive strain (blue curve), while the GaInAsSbBi (red curve) is slightly more compressive at -54” due to the incorporation of 0.13% Bi. The tetragonal distortion inferred from the measured strain is used to determine the As and Sb mole

fractions of the samples, given the calibrated group-III fluxes and Bi mole fraction from Rutherford backscattering, resulting in alloy compositions of $Ga_{0.029}In_{0.971}As_{0.882}Sb_{0.118}$ in the quaternary and $Ga_{0.029}In_{0.971}As_{0.883}Sb_{0.116}Bi_{0.001}$ in the quinary. Despite the small degree of strain observed, the 1 μm thick samples are still well within the critical thickness, and exhibit high structural and interface quality as evidenced by the Pendellösung fringes in both the quaternary $Ga_{0.029}In_{0.971}As_{0.882}Sb_{0.118}$ and quinary $Ga_{0.029}In_{0.971}As_{0.883}Sb_{0.116}Bi_{0.001}$. In contrast, the $InAs_{0.911}Sb_{0.081}Bi_{0.008}$ sample grown at 360 ºC in Ref. [1] is still closely lattice-matched with slightly greater compressive strain at -81" (green curve), however the Pendellösung fringes are characteristic of only the cap layer of the sample.

A comparison of the Bi mole fractions in the Ga-free quaternary $InAs_{0.911}Sb_{0.081}Bi_{0.008}$ grown at 360 ºC and quinary $Ga_{0.029}In_{0.971}As_{0.883}Sb_{0.116}Bi_{0.001}$ grown at 400 ºC provide only marginal evidence for the enhanced Bi incorporation efficiency in the presence of Ga. Detailed analysis of the Bi incorporation in InAsSbBi as a function of growth temperature indicates that the Bi sticking coefficient decreases with increasing growth temperature with a characteristic slope of 20.56 ºC. [27] Thus the 40 ºC increase in growth temperature should result in a factor of 0.14 reduction in Bi incorporation coefficient, resulting in an expected 0.11% Bi in an equivalent InAsSbBi alloy grown at 400 ºC. Rutherford backscattering analysis shows that the Bi mole fraction is 0.13% ± 0.02% in the quinary $Ga_{0.029}In_{0.971}As_{0.883}Sb_{0.116}Bi_{0.001}$ (see Fig. 6 inset), indicating that if Ga enhances the Bi incorporation efficiency, then the 2.9% Ga flux used in this sample was too low to conclusively observe the effect. This finding suggests future growths with higher Ga concentrations should be investigated.

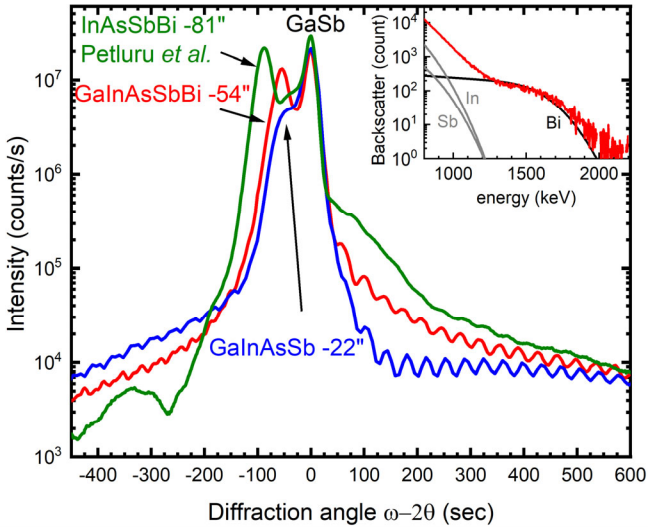

Figure 6. X-ray diffraction of quaternary $InAs_{0.911}Sb_{0.0.081}Bi_{0.008}$ (green), quaternary $Ga_{0.029}In_{0.971}As_{0.882}Sb_{0.118}$ (blue), and quinary $Ga_{0.029}In_{0.971}As_{0.883}Sb_{0.116}Bi_{0.001}$ (red). Inset shows Rutherford backscattering spectroscopy of the $Ga_{0.029}In_{0.971}As_{0.883}Sb_{0.116}Bi_{0.001}$ sample (red) and simulated fit of Bi mole fraction (black)

Steady-state photoluminescence is measured from the GaInAsSb(Bi) samples using a Bruker 80V Fourier transform infrared spectrometer and a 785 nm wavelength pump laser. Double modulation is utilized to increase the signal to noise ratio, with the laser modulated at 50 kHz. [5] The steady-state 120 K photoluminescence spectra of the GaInAsSb(Bi) samples are shown in Fig. 7 along with the quaternary $InAs_{0.911}Sb_{0.081}Bi_{0.008}$ sample for comparison. The red curve in Fig. 7 corresponds to the $Ga_{0.029}In_{0.971}As_{0.883}Sb_{0.116}Bi_{0.001}$ sample grown with the same growth conditions as the quaternary $Ga_{0.029}In_{0.971}As_{0.882}Sb_{0.118}$ alloy (blue curve), but with Bi introduced during growth. The 6 meV red shift in the rising edge of the photoluminescence is consistent with the measured 0.13% Bi mole fraction measured by Rutherford backscattering (Fig 6 inset), and results in a cutoff wavelength identical to $InAs_{0.911}Sb_{0.081}Bi_{0.008}$ due to the latter's lower Sb content. However, the photoluminescence signal of the quinary $Ga_{0.029}In_{0.971}As_{0.883}Sb_{0.116}Bi_{0.001}$ is brighter (~9% higher integrated photoluminescence intensity) than that of the quaternary $InAs_{0.911}Sb_{0.081}Bi_{0.008}$ grown at 360 ºC (0.12 µs [1]), affirming the benefit of utilizing a higher growth temperature.

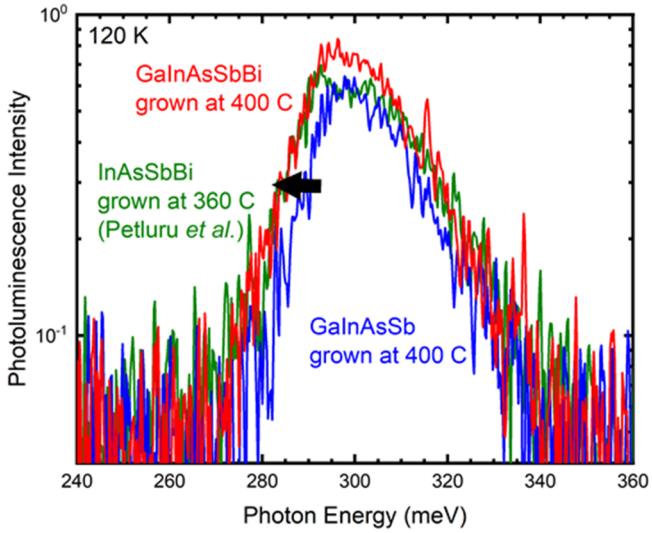

Figure 7. Photoluminescence spectra of quaternary $InAs_{0.911}Sb_{0.0.081}Bi_{0.008}$ (green), quaternary $Ga_{0.029}In_{0.971}As_{0.882}Sb_{0.118}$ (blue), and quinary $Ga_{0.029}In_{0.971}As_{0.883}Sb_{0.116}Bi_{0.001}$ (red). The black arrow indicates the 6 meV red shift of the photoluminescence signal due to the incorporation of Bi in the quinary, which emits at the same cutoff as $InAs_{0.911}Sb_{0.0.081}Bi_{0.008}$ grown under similar flux conditions at a lower temperature. The red and blue curves are from this work and the green curve is Sample D from Ref. [1]

The temperature dependent minority carrier lifetime of the quaternary and quinary alloys is measured using time-resolved photoluminescence. The GaInAsSb(Bi) samples are pumped with a 1535 nm (0.81 eV) pulsed laser with samples mounted in a liquid nitrogen cooled cryostat. The laser pulses are 3.5 ns long and the excitation is varied to inject 10^{11} – 10^{12} photons/cm^2 per pulse into the GaInAsSb(Bi) active region using a motorized half-waveplate compensator and polarizing beam splitter combination. The photoluminescence signal is collected and collimated with a 2 inch diameter f/2 90º off-axis parabolic mirror and then focused with a second off-axis parabolic mirror,

transmitted through a 2.4 μm cutoff long-pass filter, and measured by a 6 μm cutoff VIGO Systems PVI-4TE detector. A Teledyne Lecroy HD 4096 oscilloscope averages 100,000 time-resolved photoluminescence decays to acquire one photoluminescence decay signal per excitation condition per temperature from 77 to 300 K. An optical schematic of the system can be found in Ref. [28].

The excitation conditions are selected to establish low-injection conditions in the samples. Supposing all the photoexcited electron-hole pairs distribute across the 1 μm active region absorber, then the lowest excitation of 10^{11} photons/cm^2 per pulse reaching the absorber results in an initial carrier density of 10^{15} electron-hole pairs/cm^3. This is just higher than the mid-high 10^{14} cm^{-3} background carrier density determined by the recombination rate analysis in the materials indicating low-injection conditions are quickly established after the initial excitation. As the excitation level is increased, non-single exponential decay is observed at short time scales, indicating high injection conditions and a corresponding transient reduction of the lifetime. However, even in the high injection case, after the short transient of non-single exponential decay, the system returns to low-injection behavior with a characteristic slope consistent with low-injection pumping.

The minority carrier lifetime is determined as a function of temperature by fitting the characteristic slope of low-injection regime photoluminescence signal with a single exponential decay. Fig. 8 shows the time-resolved photoluminescence decays for the quaternary $Ga_{0.029}In_{0.971}As_{0.882}Sb_{0.118}$ and quinary $Ga_{0.029}In_{0.971}As_{0.883}Sb_{0.116}Bi_{0.001}$ samples under low excitation conditions at 117 K. The black curves are the photoluminescence decay data, while the subset of gray points show the data used to fit the single exponential slope in the low excitation range. The red and blue dashed lines are the best fit exponential slopes for the quinary and quaternary, respectively. It can be seen by the photoluminescence signals and slope fits that the quinary $Ga_{0.029}In_{0.971}As_{0.883}Sb_{0.116}Bi_{0.001}$ has a longer minority carrier lifetime (0.34 μs) than the quaternary (0.09 μs).

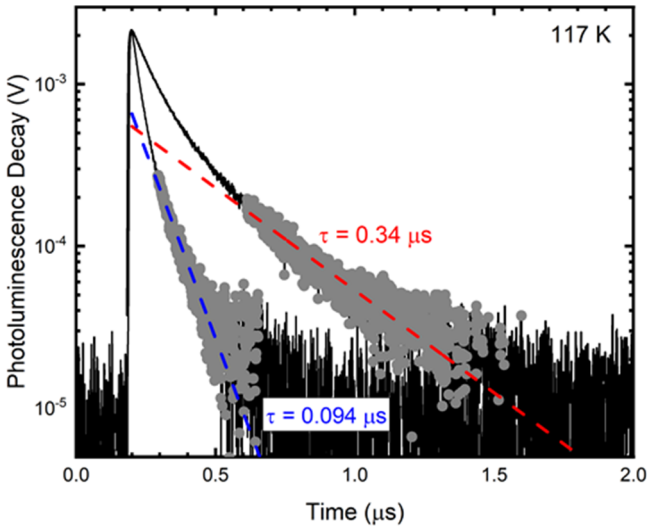

Figure 8. Time-resolved photoluminescence at low excitation conditions for $Ga_{0.029}In_{0.971}As_{0.882}Sb_{0.118}$ and $Ga_{0.029}In_{0.971}As_{0.883}Sb_{0.116}Bi_{0.001}$ at 117 K. The black curves are the photoluminescence decay data while the subset of gray points show the data used to fit the region of single exponential decay. The red and blue dashed lines show the resulting slope fit for the quinary and quaternary, respectively. The decay rates of the exponential slope correspond to the minority carrier lifetimes

The recombination rate analysis is performed on the GaInAsSb(Bi) samples by fitting the three recombination rate mechanisms to the temperature dependent minority carrier lifetime determined by,

$$\frac{1}{\tau_{mc}} = \frac{1}{\phi\tau_{rad}} + \frac{1}{\tau_{SRH}} + \frac{1}{\tau_{Auger}} \quad (4)$$

In Eq. (4), the minority carrier lifetime τ_{mc} is modeled as a function of the radiative lifetime τ_{rad} scaled by the photon recycling factor ϕ, the Shockley-Read-Hall (SRH) lifetime τ_{SRH} and the Auger lifetime τ_{Auger}. Further description of the recombination rate analysis can be found in Ref. [29] and references therein.

Fig. 9 shows the temperature dependent minority carrier lifetime of the samples grown in this study alongside the solid curves showing the resultant recombination rate fit in Eq. (4). The temperature-dependent minority carrier lifetime of the quaternary $Ga_{0.029}In_{0.971}As_{0.882}Sb_{0.118}$ (circles and blue curve) is lower than the quinary $Ga_{0.029}In_{0.971}As_{0.883}Sb_{0.116}Bi_{0.001}$ (squares and red curve). This could be due to the intrinsic defects introduced in the InAsSb ternary by adding Ga into the system. [30] Once Bi is introduced in the quinary growth, however, the minority carrier lifetime increases by >3× in the SRH-limited regime, possibly a result of the surfactant behavior of Bi, [31,32] an additional benefit of Bi being introduced during growth.

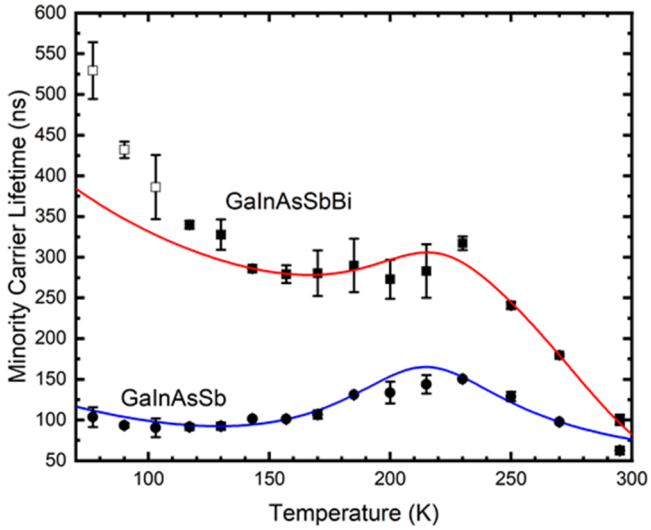

Figure 9. Temperature dependent minority carrier lifetime of the GaInAsSb(Bi) samples. The circles and blue curve correspond to the data and model fit for the quaternary $Ga_{0.029}In_{0.971}As_{0.882}Sb_{0.118}$ and the squares and red curve are the data and model fit for quinary $Ga_{0.029}In_{0.971}As_{0.883}Sb_{0.116}Bi_{0.001}$. The empty squares are the data points excluded from the fit for the quinary

The 0.34 µs lifetime observed in the quinary grown at 400 ºC is consistent with the trends in Ref. [9], where the lifetime in the InAsSbBi alloys grown in the same molecular beam epitaxy system is consistently just under the expectation for lattice-matched $InAs_{0.91}Sb_{0.09}$ (0.39 µs at 400 ºC). While the conclusions that can be drawn from comparisons of material quality metrics like minority carrier lifetime in samples grown at different times are typically limited, careful periodic benchmarking of the lifetime of material produced by this molecular beam epitaxy system enables the comparisons here. The minority carrier lifetime of a mid-wave infrared InAs/InAsSb superlattice benchmark structure has been carefully tracked over time, and is comparable at a Shockley-Read-Hall-limited lifetime of 2 µs during the growth campaigns which produced the GaInAsSb(Bi) samples examined here as well as the Ga-free $InAs_{0.911}Sb_{0.081}Bi_{0.008}$ sample from Ref [9]. This indicates that the state of the molecular beam epitaxy system and quality of the mid-wave infrared InAsSb-based material produced in these time frames is comparable.

Table 5 provides the best-fit parameters to the temperature dependent minority carrier lifetime. The majority carrier concentration determined by a recombination rate analysis of the time-resolved photoluminescence becomes increasingly less sensitive as the majority carrier concentration decreases (particularly in undoped samples), however, this approach is sufficient for the purposes of this report. [29,33] The defect levels of both samples seem to be shallow toward the conduction band. The defect cross-section-concentration product is consistent with the observed minority carrier lifetime increase in the quinary GaInAsSbBi sample, further highlighting that Bi may have aided in growing a higher quality material with fewer defects. The Bloch overlap parameter $|F_1F_2|$ typically has large influence on the minority carrier lifetime at higher temperatures where the Auger

recombination intrinsically dominates. However, the fact that the minority carrier lifetime of the quaternary GaInAsSb is heavily dominated by the SRH recombination could suggest that the model is less sensitive to the Bloch overlap parameter in these samples.

Table 5. Best fit parameters extracted from a recombination rate analysis on the temperature dependent minority carrier lifetime of the GaInAsSb(Bi) samples grown

Sample	Type	Majority Carrier Concentration (cm^{-3})	$E_c - E_t$ (meV)	σN_t (10^{-2} cm^{-1})	$\lvert F_1 F_2 \rvert$
GaInAsSb	*n*-type	6.08×10^{14}	73.9	86.3	0.0699
GaInAsSbBi	*n*-type	8.60×10^{14}	96.6	24.3	0.4674

5.0 CONCLUSIONS

More growth and minority carrier lifetime studies are required to further understand the benefits of adding Ga and understand its relationship with Bi incorporation efficiency. Evaluation of the photoluminescence spectra and time-resolved photoluminescence decays show that Bi extends the cutoff of GaInAsSb to longer wavelengths, and results in improved minority carrier lifetime in quinary GaInAsSbBi. InAsSbBi can achieve the same cutoff wavelength, but requires higher Bi mole fractions achieved with lower temperature growth conditions that degrade its minority carrier lifetime. The findings presented here provide evidence that the inclusion of Ga in quinary GaInAsSbBi may be the enabling factor to achieve long minority carrier lifetime mid-wave infrared material, however whether or not Ga significantly modifies the Bi sticking coefficient remains to be determined.

6.0 REFERENCES

[1] P. Petluru, P.C. Grant, A.J. Muhowski, I.M. Obermeier, M.S. Milosavljevic, S.R. Johnson, D. Wasserman, E.H. Steenbergen, P.T. Webster, Appl. Phys. Lett **117**, 061103, (2020).

[2] Z.R. Wasilewski, M.M. Dion, D.J. Lockwood, P. Poole, R.W. Streater, and A.J. SpringThorpe, "Composition of AlGaAs," J. of Appl. Phys. **81**, 1683, (1997).

[3] P.T. Webster, A.J. Shalindar, S.T. Schaefer, and S.R. Johnson, Appl. Phys. Lett. **111**, 082104, (2017).

[4] S.T. Schaefer, R.R. Kosireddy, P.T. Webster, and S.R. Johnson, J. of Appl. Phys. **126**, 83101, (2019).

[5] A.R. Reisinger, R.N. Roberts, S.R. Chinn, and T.H. Myers II, Rev. Sci. Instrum. **60**, 82, (1989).

[6] L.K. Casias, C.P. Morath, E.H. Steenbergen, G.A. Umana-Membreno, P.T. Webster, J.V. Logan, J.K. Kim, G. Balakrishnan, L. Faraone, S. Krishna, Appl. Phys. Lett. **116**, 182109, (2020).

[7] P.T. Webster, N.A. Riordan, S. Liu, E.H. Steenbergen, R.A. Synowicki, Y.-H. Zhang, and S.R. Johnson, J. Appl. Phys. **118**, 245706, (2015).

[8] S.R. Johnson and T. Tiedje, J. Appl. Phys. **78**, 5609, (1995).

[9] L. Viña, S. Logothetidis, and M. Cardona, Phys. Rev. B **30**, 1979, (1984).

[10] N. A. Riordan, C. Gogineni, S. R. Johnson, X. Lu, T. Tiedje, D. Ding, Y.-H. Zhang, R. Fritz, K. Kolata, S. Chatterjee, K. Volz, and S. W. Koch, J. Mater. Sci. Mater. Electron. **23**, 1799, (2012).

[11] T. M. Christian, K. Alberi, D. A. Beaton, B. Fluegel, and A. Mascarenhas, Jpn. J. Appl. Phys. **56**, 035801, (2017).

[12] A. R. Mohmad, F. Bastiman, C. J. Hunter, R. Richards, S. J. Sweeney, J. S. Ng, and J. P. R. David, Appl. Phys. Lett. **101**, 012106, (2012).

[13] G. Pettinari, A. Polimeni, M. Capizzi, J. H. Blokland, P. C. M. Christianen, J. C. Maan, E. C. Young, and T. Tiedje, Appl. Phys. Lett. **92**, 262105, (2008).

[14] E. D. Palik and R. T. Holm, "Handbook of Optical Constants of Solids," San Diego, Academic Press, 1985.

[15] B.V. Olson, E.A. Shaner, J.K. Kim, J.F. Klem, S.D. Hawkins, L.M. Murray, J.P. Prineas, M.E. Flatte, and T.F. Boggess, Appl. Phys. Lett. **101**, 092109, (2012).

[16] B.V. Olson, PhD dissertation, University of Iowa, 2013.

[17] B.V. Olson, E.A. Kadlec, J.K. Kim, J.F. Klem, S.D. Hawkins, and E.A. Shaner, Phys. Rev. Applied **3**, 044010, (2015).

[18] L. Höglund, D.Z. Ting, A. Soibel, A. Fisher, A. Khoshakhlagh, C.J. Hill, S. Keo, and S.D. Gunapala, Appl. Phys. Lett. **105**, 193510, (2014).

[19] R.A. Carrasco, C.P. Morath, J.V. Logan, K.B. Woller, P.C. Grant, H. Orozco, M.S. Milosavljevic, S. R. Johnson, G. Balakrishnan, P.T. Webster, Appl. Phys. Lett **120**, 031102, (2022).

[20] S. T. Schaefer, R. R. Kosireddy, P. T. Webster and S. R. Johnson, J. Appl. Phys. **126**, 083101, (2019).

[21] S. P. Svensson, D. Donetsky, D. Wang, H. Hier, F. J. Crowne and G. Belenky, J. Cryst. Growth, **334**, 103, (2011).

[22] P. T. Webster, N. A. Riordan, S. Liu, E. H. Steenbergen, R. A. Synowicki, Y.-H. Zhang and S. R. Johnson, Appl. Phys. Lett. **106**, 061907, (2015).

[23] V. Bahrami-Yekta, T. Tiedje and M. Masnadi-Shirazi, "MBE growth optimization for GaAsBi and dependence of photoluminescence on growth temperature," Semicond. Sci. Technol., vol. 30, p. 094007, (2015).

[24] A. Tixier, M. Adamcyk and T. Tiedje, Appl. Phys. Lett. **82**, 2245, (2003).

[25] A. Janotti, S. -H. Wei and S. B. Zhang, Phys. Rev. B. **65**, 115203, (2002).

[26] H. Li, S. Liu, O. O. Cellek, D. Ding, X.-M. Shen, E. H. Steenbergen, J. Fan, Z. Lin, Z.-Y. He, Q. Zhang, P. T. Webster, S. R. Johnson, L. Ouyang, D. J. Smith and Y.-H. Zhang, J. Cryst. Growth **378**, 145, (2013).

[27] Z. M. Fang, K. Y. Ma, R. M. Cohen and G. B. Stringfellow, J. Appl. Phys. **68**, 1187, (1990).

[28] G. D. Jenkins, C. P. Morath and V. M. Cowan, J. Electron Mater. **46**, 5405, (2017).

[29] R. A. Carrasco, C. P. Morath, P. C. Grant, G. Ariyawansa, C. A. Stephenson, C. N. Kadlec, S. D. Hawkins, J. F. Klem, E. A. Shaner, E. H. Steenbergen, S. T. Schaefer, S. R. Johnson and P. T. Webster, J. Appl. Phys. **129**, 184501, (2021).

[30] B. C. Connelly, G. D. Metcalfe, H. Shen, M. Wraback, C. J. Canedy, I. Vurgaftman, J. S. Melinger, C. A. Affouda, E. M. Jackson, J. A. Nolde, J. R. Meyer and E. H. Aifer, J. Electron. Mat. **42**, 3203, (2013).

[31] P. T. Webster, N. A. Riordan, C. Gogineni, S. Liu, J. Lu, X.-H. Zhao, D. J. Smith, Y.-H. Zhang and S. R. Johnson, J. Vac. Sci. Technol. B **32**, 02C120, (2014).

[32] P. T. Webster, S. T. Schaefer, E. H. Steenbergen and S. R. Johnson, Proc. SPIE **10540**, 105401E, (2018).

[33] R. A. Carrasco, J. George, D. Maestas, Z. M. Alsaad, D. Garnham, C. P. Morath, J. M. Duran, G. Ariyawansa and P. T. Webster, J. Appl. Phys. **130**, 114501, (2021).

PUBLICATIONS AND PRESENTATIONS

Peer-Reviewed Journal Articles

1. R.A. Carrasco, C.P. Morath, J.V. Logan, K.B. Woller, P.C. Grant, H. Orozco, M.S. Milosavljevic, S. R. Johnson, G. Balakrishnan, P.T. Webster, "Photoluminescence and minority carrier lifetime of quinary GaInAsSbBi grown on GaSb by molecular beam epitaxy," Appl. Phys. Lett, vol. 120, pp. 031102, Jan. 2022.
    - DOI: https://doi.org/10.1063/5.0078809.
2. P. Petluru, P.C. Grant, A.J. Muhowski, I.M. Obermeier, M.S. Milosavljevic, S.R. Johnson, D. Wasserman, E.H. Steenbergen, P.T. Webster, "*Minority carrier lifetime and photoluminescence of mid-wave infrared InAsSbBi*," Appl. Phys. Lett, vol. 117, pp. 061103, Aug. 2020.
    - DOI: https://doi.org/10.1063/5.0064043
3. L.K. Casias, C.P. Morath, E.H. Steenbergen, G.A. Umana-Membreno, P.T. Webster, J.V. Logan, J.K. Kim, G. Balakrishnan, L. Faraone, S. Krishna, "*Vertical carrier transport in strain-balanced InAs/InAsSb type-II superlattice material*," Appl. Phys. Lett., vol. 116, pp. 182109, May 2020.
    - DOI: https://doi.org/10.1063/1.5144079

Conference Presentations (Selected)

1. R.A. Carrasco, P.C. Grant, H. Orozco, M.S. Milosavljevic, C.P. Morath, S.R. Johnson, P.T. Webster, "Photoluminescence and Minority Carrier Lifetime of Quinary GaInAsSbBi Alloys Grown by Molecular Beam Epitaxy," *21st International Conference on Molecular Beam Epitaxy*, Puerta Vallarta, Mexico, Sep. 2021.
2. S.T. Schaefer, M.S. Milosavljevic, P.T. Webster, S.R. Johnson, "*Temperature and Excitation Dependent Photoluminescence Measurements of Nonradiative Lifetime in InAs(SbBi)*," *15th International Conference on Mid-Infrared Optoelectronic Materials and Devices*, Surrey, United Kingdom, Sep. 2021.
3. P.T. Webster, R.A. Carrasco, D. Garnham, J. George, P.C.Grant, C.P. Morath, D. Maestas, "Minority Carrier Lifetime of Strain-Balanced InGaAs/InAsSb Superlattices & Associated Detector Performance Gains in Mid-Wave Infrared Space Applications," *American Physical Society March Meeting*, Virtual Conference, Mar. 2021.
4. P.T. Webster, P. Petluru, P.C. Grant, A.J. Muhowski, I.M. Obermeier, M.S. Milosavljevic, S.R. Johnson, D. Wasserman, E.H. Steenbergen, "Minority Carrier Lifetime and Photoluminescence of Mid-Wave Infrared InAsSbBi," *2020 Government Focal Plane Array Technical Workshop*, Chantilly VA, Feb. 2020.

DISTRIBUTION LIST

DTIC/OCP 8725 John J. Kingman Rd, Suite 0944 Ft Belvoir, VA 22060-6218	1 cy
AFRL/RVIL Kirtland AFB, NM 87117-5776	1 cy
Official Record Copy AFRL/RVS/Preston Webster	1 cy